

cy.2

FEB 09 1995



STATUS REPORT ON THE CALCULATION OF BLUNT BODY FLOW FIELDS IN SUPERSONIC, NONUNIFORM FLOWS

PROPULSION WIND TUNNEL FACILITY
ARNOLD ENGINEERING DEVELOPMENT CENTER
AIR FORCE SYSTEMS COMMAND
ARNOLD AIR FORCE STATION, TENNESSEE 37389

March 1976

Final Report for Period 1 July 1974 — 30 June 1975

Approved for public release; distribution unlimited.

Property of U. S. Air Force
AEDC LIBRARY
F40600-75-C-0001

Prepared for

DIRECTORATE OF TECHNOLOGY
ARNOLD ENGINEERING DEVELOPMENT CENTER
ARNOLD AIR FORCE STATION, TENNESSEE 37389

NOTICES

When U. S. Government drawings specifications, or other data are used for any purpose other than a definitely related Government procurement operation, the Government thereby incurs no responsibility nor any obligation whatsoever, and the fact that the Government may have formulated, furnished, or in any way supplied the said drawings, specifications, or other data, is not to be regarded by implication or otherwise, or in any manner licensing the holder or any other person or corporation, or conveying any rights or permission to manufacture, use, or sell any patented invention that may in any way be related thereto.

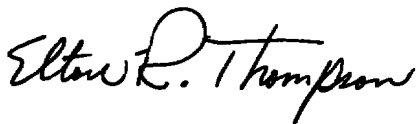
Qualified users may obtain copies of this report from the Defense Documentation Center.

References to named commercial products in this report are not to be considered in any sense as an endorsement of the product by the United States Air Force or the Government.

APPROVAL STATEMENT

This technical report has been reviewed and is approved for publication.

FOR THE COMMANDER



ELTON R. THOMPSON
Research & Development
Division
Directorate of Technology



ROBERT O. DIETZ
Director of Technology

UNCLASSIFIED

REPORT DOCUMENTATION PAGE		READ INSTRUCTIONS BEFORE COMPLETING FORM
1 REPORT NUMBER AEDC-TR-76-31	2 GOVT ACCESSION NO.	3 RECIPIENT'S CATALOG NUMBER
4 TITLE (and Subtitle) STATUS REPORT ON THE CALCULATION OF BLUNT BODY FLOW FIELDS IN SUPERSONIC, NONUNIFORM FLOWS	5 TYPE OF REPORT & PERIOD COVERED Final Report, 1 July 1974 - 30 June 1975	
	6 PERFORMING ORG. REPORT NUMBER	
7 AUTHOR(s) Harold J. Schmidt, ARO, Inc.	8 CONTRACT OR GRANT NUMBER(s)	
9 PERFORMING ORGANIZATION NAME AND ADDRESS Arnold Engineering Development Center (DY) Air Force Systems Command Arnold Air Force Station, TN 37389	10 PROGRAM ELEMENT, PROJECT, TASK AREA & WORK UNIT NUMBERS Program Element 65807F	
11 CONTROLLING OFFICE NAME AND ADDRESS Arnold Engineering Development Center (DYFS), Air Force Systems Command, Arnold Air Force Station, TN 37389	12 REPORT DATE March 1976	
	13. NUMBER OF PAGES 35	
14 MONITORING AGENCY NAME & ADDRESS (if different from Controlling Office)	15 SECURITY CLASS. (of this report) UNCLASSIFIED	
	15a. DECLASSIFICATION/DOWNGRADING SCHEDULE N/A	
16 DISTRIBUTION STATEMENT (of this Report) Approved for public release; distribution unlimited.		
17 DISTRIBUTION STATEMENT (of the abstract entered in Block 20, if different from Report)		
18 SUPPLEMENTARY NOTES Available in DDC.		
19 KEY WORDS (Continue on reverse side if necessary and identify by block number) <div style="display: flex; justify-content: space-between;"> <div> nonuniform flow supersonic flow blunt bodies </div> <div> fluid flow computations </div> </div>		
20 ABSTRACT (Continue on reverse side if necessary and identify by block number) It is difficult to eliminate flow nonuniformities in facilities for the testing of ablative heat shield materials. To investigate the potential effects of free-stream nonuniformities, a modification of an existing analytical method developed by Moretti and co-workers for uniform blunt body flows has been used. The results of the study indicate that for the flow model used, the free-stream nonuniformity can significantly alter the flow properties of the body surface. In particular, free-stream Mach number gradients		

UNCLASSIFIED

UNCLASSIFIED

20. ABSTRACT (Continued)

can result in velocity gradients at the body surface which, in turn, will influence local heating rates.

UNCLASSIFIED

PREFACE

The work reported herein was conducted by the Arnold Engineering Development Center (AEDC), Air Force Systems Command (AFSC), under Program Element 65807F. The results of the research were obtained by ARO, Inc. (a subsidiary of Sverdrup & Parcel and Associates, Inc.), contract operator of AEDC, AFSC, Arnold Air Force Station, Tennessee, under ARO Project No. P33A-36A. The author of this report was Harold J. Schmidt, ARO, Inc. The manuscript (ARO Control No. ARO-PWT-TR-75-109) was submitted for publication on June 30, 1975.

CONTENTS

	<u>Page</u>
1.0 INTRODUCTION	5
2.0 OUTLINE OF THE METHOD	
2.1 Field Point Computations	9
2.2 Shock Points	15
2.3 Body Points	19
2.4 Outer Boundary	21
3.0 RESULTS OF SAMPLE CALCULATIONS	21
4.0 CONCLUSIONS	31
REFERENCES	33

ILLUSTRATIONS

Figure

1. Flow Geometry and Coordinate System Definition Used in the Analysis of Blunt Body Flow with a Nonuniform Free Stream	7
2. Computational Regions in the Physical Space and the Continuous and Discretized Transformed Space	8
3. Diagram of Geometry of the Shock Boundary Calculation in the Two-Dimensional Case or a Symmetry Plane Calculation in the Three-Dimensional Case	16
4. Shock Path in the Quasi-One-Dimensional Unsteady Flow Plane Showing the Three Characteristic Directions	18
5. Body Path in the Quasi-One-Dimensional Unsteady Flow Plane Showing the Three Characteristic Directions with the Condition that $\bar{u} = 0$ at the Body Surface	20
6. Three-Dimensional Flow Field for an 8-deg Sphere Cone at 3 deg Angle of Attack in a Mach Number 7.0 Uniform Flow	23
7. Nonuniform Free-Stream Model Used to Illustrate Effects of a Radially Increasing Flow Mach Number	24

<u>Figure</u>	<u>Page</u>
8. Calculated Shock Shape for a Nonuniform Free-Stream Flow in Which the Mach Number Radially Increases	25
9. Calculated Static Pressure Distributions for a Uniform Free Stream and Nonuniform Free Stream in Which the Mach Number Radially Increases	26
10. Calculated Flow Velocities Near the Body Stagnation Point for a Uniform Free Stream and a Nonuniform Free Stream in Which the Mach Number Radially Increases	27
11. Nonuniform Free-Stream Model Used to Illustrate Effects of a Radially Decreasing Flow Mach Number	28
12. Calculated Shock Shape for a Nonuniform Free-Stream Flow in Which the Mach Number Radially Decreases	29
13. Calculated Static Pressure Distributions for a Uniform Free Stream and a Nonuniform Free Stream in Which the Mach Number Radially Decreases	30
14. Calculated Flow Velocities near the Body Stagnation Point for a Uniform Free Stream and a Nonuniform Free Stream in Which the Mach Number Radially Decreases	31
NOMENCLATURE	35

1.0 INTRODUCTION

Simulation of conditions in ground testing of high performance reentry vehicles continues to be a formidable task. The high heating rates and pressure levels achieved in flight tests are difficult to duplicate in ground tests, where not only the test model but the test equipment as well must withstand the environment. To date, the arc heater has been the most successful device for producing an environment for testing ablative materials for reentry vehicles. However, the arc heater has disadvantages in that the flow Mach number is low, the plasma jet enthalpy distribution is nonuniform, and testing is limited to small models. One method used to extend the utility of the arc heater is to envelop the arc heater flow with a uniform, high Mach number, low enthalpy flow (i. e., a cold shroud). The concept is that the high enthalpy flow from the arc will be injected into the boundary layer around the model and will correctly simulate the heating rates while the surrounding high Mach number cold flow will provide the correct pressure distribution simulation on the model.

Whether conventional or shrouded, the arc heaters in current use produce nonuniform though axially symmetric test jets. To confidently apply data from such a test to the design of considerably scaled-up flight vehicles, one must ascertain the influence of the flow nonuniformities. The object of the present effort is to extend existing analytical techniques for blunt body flow-field analysis to include the effects of the nonuniform free stream.

The most successful analytical method existing was developed by Moretti and his co-workers (Refs. 1 through 3). This is a time-dependent technique in which the blunt body flow-field solution is taken to be the asymptotic limit of an unsteady flow in which steady-state boundary conditions are imposed. The Moretti technique differs in two significant aspects from other methods of this same general class. First, the Moretti technique is direct, with the body shape specified and the shock shape calculated as part of the solution, and second, the shock wave is treated as a discontinuity located at the upstream boundary of the computational region.

There are several versions of the Moretti program in use, and the versions differ by the geometry considered, the main coordinate systems employed, and the particular computer for which they were written. For this study, two of these automated versions were used.

The first is a simple model applicable to axisymmetric blunt bodies at zero angle of attack. This version used a combination of two-dimensional cartesian and polar coordinate systems. Due to its relative simplicity, this program was used to gain familiarity with the Moretti technique and to perform preliminary calculations with a nonuniform free stream. The second version of the program is for an axisymmetric body at angle of attack and uses a spherical coordinate system. This second version, as obtained from Sandia Corporation, was written for a CDC 6600 computer and included real gas effects. When this version was converted to the IBM system, the real gas capability was deleted in order to reduce the storage requirements and running time.

While both of these programs have a capability of extending the computations downstream of the nose region into the supersonic flow field, this option was not exercised. This extension is quite straightforward but does require reprogramming to redefine the variables. The nose region of the blunt body, however, is of primary interest in regard to the intended application, and this effort has concentrated on calculating this flow field. Also, since the zero angle of attack is a special case of a more general angle-of-attack calculation, only the general case will be considered here.

In Section 2.0, the method is outlined. In Section 3.0, the results of the sample computations are presented. In Section 4.0, the principal conclusions, limitations, and possible extensions of the analysis are discussed. In particular, the results indicate that flow nonuniformities can alter the heating rates to the extent that they must be taken into account when scaling experimental data for different sized models.

2.0 OUTLINE OF THE METHOD

The flow geometry incorporated in the blunt body program with a nonuniform free stream is shown in Fig. 1. For simplicity, the body shape is taken to be an axisymmetric, spherically blunt cone. While the program is written for axisymmetric conical shapes, in principle, the body need only be planar symmetric in the pitch plane, and the blunt nose does not have to be spherical. The primary spherical coordinate system is located on the body axis and is aligned with respect to the wind vector. The origin of the coordinate system is

neither fixed nor required to be at the center of curvature of the blunt nose. However, as a fundamental assumption, the free-stream stagnation streamline is taken to be defined by the wind vector passing through the coordinate origin. For a spherical nose at small angles of attack, with the sonic surface occurring in the nose region, this is a reasonable approximation. In the spherical coordinate system, the body centerline and the x and z axes are in the same plane. The meridian angle, ϕ , which has values between 0 and π in the leeward and windward planes, respectively, is measured in the x - y plane, which is orthogonal to the x - z plane. The azimuthal angle, θ (measured in the r - z plane), is normally confined to the range $\pi/2 < \theta < \pi$ but can be further restricted for a particular problem. Note that when the appellations "meridian" and "azimuth" are applied to the coordinate angles, it is the coordinate system that is referenced and not directions on the body surface.

The free-stream flow is taken to be parallel with a uniform static pressure. The velocity and density in the free stream are taken to have axially symmetric profiles with respect to the previously defined stagnation line, which is an extension of the coordinate system baseline. The distribution of the velocity is depicted in Fig. 1.

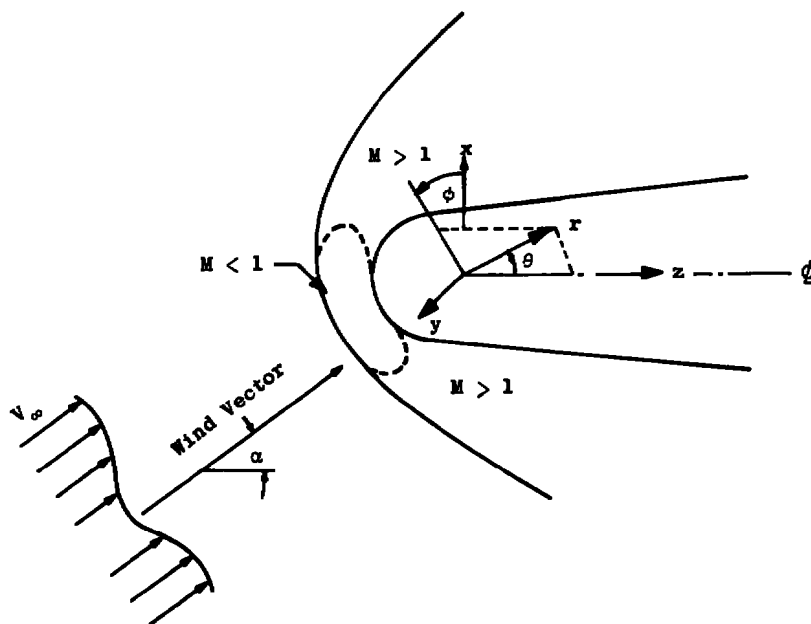
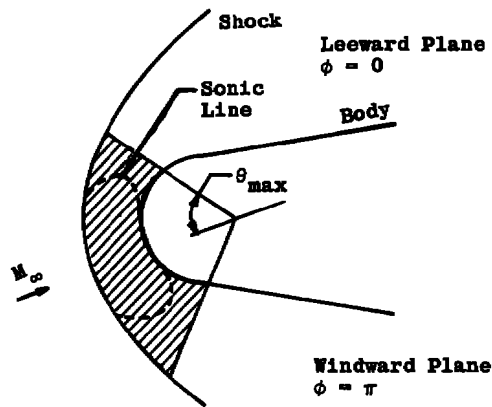
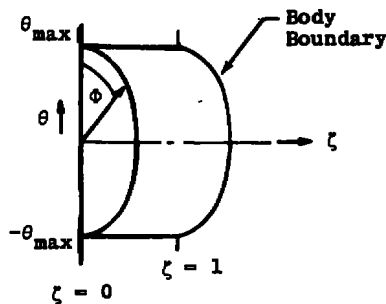


Figure 1. Flow geometry and coordinate system definition used in the analysis of blunt body flow with a nonuniform free stream.

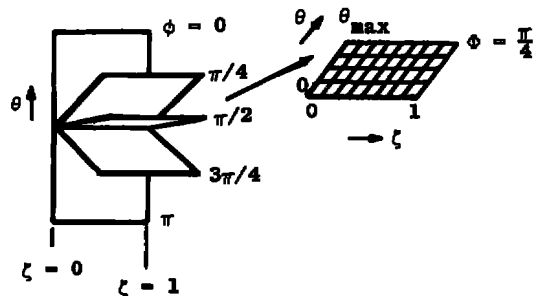
The actual flow computational region of interest in the blunt body problem is the region between the bow shock wave, the shape and position of which are determined as part of the solution, and the specified body surface. Closure of the computational region is provided by the specification of a limiting value of the azimuth angle, θ_{\max} . This angle is selected in conjunction with the placement of the coordinate origin such that the flow through this closure surface is everywhere supersonic. That is, the subsonic flow in the stagnation region of the blunt body must be wholly embedded within the computational region. The computational region in the physical space is depicted in Fig. 2a. The solution on the closure surface, or immediately below it, will permit the continuation of the flow-field calculation further downstream using conventional steady-state analytical methods such as the method of characteristics.



a. Calculational region in physical space



b. Computational region in transformed space



c. Discretized computational regions in transformed space

Figure 2. Computational regions in the physical space and the continuous and discretized transformed space.

The basic concept is to consider the time-dependent equations of motion for an inviscid fluid within the outlined region of interest. In a steady-state formulation of the problem, the describing equations in the subsonic regions of the flow are elliptic, and the problem would be an elliptic boundary value problem with unknown free boundaries, namely the shock and sonic surfaces. In the unsteady formulation the appropriate flow equations are hyperbolic in character over the entire flow region, and the problem can be formulated as an initial value problem, which is not as difficult a computational problem. While the body surface is fixed in time, the boundary represented by the shock surface is allowed to move, and in essence it is the asymptotic time position of the shock wave which represents the final solution. The calculations in the interior of the flow field are different from those performed at the boundaries, and each of these calculations will be considered separately in the following subsections.

2.1 FIELD POINT COMPUTATIONS

With u_θ , u_r , and u_ϕ representing the velocity components in the spherical coordinate directions, the governing system of non-steady flow equations for an inviscid, nonconducting, perfect gas is given as

$$\frac{\partial p}{\partial t} + \frac{\partial}{\partial r}(\rho u_r) + \frac{2}{r} \rho u_r + \frac{1}{r \sin \theta} \frac{\partial}{\partial \phi}(\rho u_\phi) + \frac{\rho u_\theta}{r \tan \theta} + \frac{1}{r} \frac{\partial}{\partial \theta}(\rho u_\theta) = 0 \quad (1)$$

$$\frac{\partial u_r}{\partial t} + u_r \frac{\partial u_r}{\partial r} + \frac{u_\theta}{r} \frac{\partial u_r}{\partial \theta} + \frac{u_\phi}{r \sin \theta} \frac{\partial u_r}{\partial \phi} - \frac{(u_\theta^2 + u_\phi^2)}{r} + \frac{1}{\rho} \frac{\partial p}{\partial r} = 0 \quad (2)$$

$$\frac{\partial u_\theta}{\partial t} + u_r \frac{\partial u_\theta}{\partial r} + \frac{u_\theta}{r} \frac{\partial u_\theta}{\partial \theta} + \frac{u_\phi}{r \sin \theta} \frac{\partial u_\theta}{\partial \phi} + \frac{u_r u_\theta}{r} + \frac{u_\phi^2}{r} \cot \theta + \frac{1}{\rho r} \frac{\partial p}{\partial \theta} = 0 \quad (3)$$

$$\begin{aligned} \frac{\partial u_\phi}{\partial t} + u_r \frac{\partial u_\phi}{\partial r} + \frac{u_\theta}{r} \frac{\partial u_\phi}{\partial \theta} + \frac{u_\phi}{r \sin \theta} \frac{\partial u_\phi}{\partial \phi} + \frac{u_r u_\phi}{r} \\ - \frac{u_\phi u_\theta}{r} \cot \theta + \frac{1}{\rho r \sin \theta} \frac{\partial p}{\partial \phi} = 0 \end{aligned} \quad (4)$$

$$\frac{\partial s}{\partial t} + u_r \frac{\partial s}{\partial r} + \frac{u_\phi}{r \sin \theta} \frac{\partial s}{\partial \phi} + \frac{1}{r} u_\theta \frac{\partial s}{\partial \theta} = 0 \quad (5)$$

where ρ is the static density, p the static pressure, and s is the entropy. The first equation is the continuity equation, followed by the three Euler equations, and the final equation expresses the fact that the entropy is constant along the streamlines. In view of the complex geometry involved in the flow field and the fact that there is no length scale associated with an inviscid flow, it is convenient to transform the independent variables and nondimensionalize the dependent variables in the above equations.

To transform the independent variables, one can take the body surface as an explicitly defined function, B , which is dependent on the azimuth angle and meridian angles only. The body surface is defined by an equation of the form

$$r - B(\phi, \theta) = 0 \quad (6)$$

A similar relation can be defined for the shock wave surface as

$$r - S(\phi, \theta, t) = 0 \quad (7)$$

where the function S is implicit and also functionally time dependent since the shock is allowed to have a radial motion. With δ representing the distance between the body and shock surfaces along any radius, this distance is given as

$$\delta(\phi, \theta, t) = S - B \quad (8)$$

A transformation of variables can then be defined by

$$\zeta = \frac{r - B}{\delta}, \quad \Theta = \theta, \quad \Phi = \phi, \quad T = t \quad (9)$$

where ζ , Θ , Φ , and T are the new independent variables. Under this transformation the physical space of Fig. 2a can be considered to map into the space of Fig. 2b where the shock surface boundary lies in the plane $\zeta = 1$ and the body surface lies in the plane $\zeta = 0$. The required transformation relations are given as

$$\frac{\partial}{\partial r} = \frac{1}{\delta} \frac{\partial}{\partial \zeta}$$

$$\frac{\partial}{\partial \theta} = \frac{C(\theta)}{\delta} \frac{\partial}{\partial \zeta} + \frac{\partial}{\partial \Theta}$$

$$\begin{aligned}\frac{\partial}{\partial \phi} &= -\frac{C(\Phi)}{\delta} \frac{\partial}{\partial \zeta} + \frac{\partial}{\partial \Phi} \\ \frac{\partial}{\partial t} &= -\frac{\zeta}{\delta} \frac{\partial S}{\partial t} \frac{\partial}{\partial \zeta} + \frac{\partial}{\partial T}\end{aligned}\quad (10)$$

with the function $C(x)$ being defined as

$$C(x) = \frac{\partial B}{\partial x} (1 - \zeta) + \zeta \frac{\partial S}{\partial x} \quad (11)$$

where x is a dummy notation representing either ϕ or θ as the case may be. With the establishment of the transformation relations, the original notations θ , ϕ , and t will be retained for the transformed variables to which they are identical.

To nondimensionalize the dependent variables, it is convenient to use the free-stream static pressure and free-stream density on the principal coordinate axis. The following nondimensional variables are introduced:

Pressure	$P = \ln(p/p_\infty)$	
Density	$R = \ln(\rho/\rho_\infty)$	
Entropy	$E = P - \gamma R$	
Velocity	$(u, v, w) = (u_r, u_\theta, u_\phi) / \sqrt{(p_\infty/\rho_\infty)} \zeta$	(12)

A convenient reference length is taken as the body nose radius, and the reference time unit is taken as $r_n / \sqrt{(p_\infty/\rho_\infty)} \zeta$

Incorporating the transformation relation, Eq. (10), and the non-dimensionalizations, Eq. (12), into the governing system, Eqs. (1) through (5), yields the following coupled system of equations.

$$\begin{aligned}-\frac{\partial P}{\partial t} &= a_0 \frac{\partial P}{\partial \theta} + a_1 \frac{\partial P}{\partial \phi} + a_2 \frac{\partial P}{\partial \zeta} + a_3 \frac{\partial u}{\partial \zeta} + a_4 \frac{\partial v}{\partial \theta} + a_5 \frac{\partial v}{\partial \zeta} \\ &+ a_6 \frac{\partial w}{\partial \phi} - a_7 \frac{\partial w}{\partial \zeta} + a_8\end{aligned}\quad (13)$$

$$-\frac{\partial u}{\partial t} = a_0 \frac{\partial u}{\partial \theta} + a_1 \frac{\partial u}{\partial \phi} + a_2 \frac{\partial u}{\partial \zeta} + a_9 \frac{\partial P}{\partial \zeta} + a_{10} \quad (14)$$

$$\frac{-\partial v}{\partial t} = a_0 \frac{\partial v}{\partial \theta} + a_1 \frac{\partial v}{\partial \phi} + a_2 \frac{\partial v}{\partial \zeta} + a_{11} \frac{\partial P}{\partial \theta} + a_{12} \frac{\partial P}{\partial \zeta} + a_{13} \quad (15)$$

$$\frac{-\partial w}{\partial t} = a_0 \frac{\partial w}{\partial \theta} + a_1 \frac{\partial w}{\partial \phi} + a_2 \frac{\partial w}{\partial \zeta} + a_{14} \frac{\partial P}{\partial \phi} + a_{15} \frac{\partial P}{\partial \zeta} + a_{16} \quad (16)$$

$$\frac{-\partial E}{\partial t} = a_0 \frac{\partial E}{\partial \theta} + a_1 \frac{\partial E}{\partial \phi} + a_2 \frac{\partial E}{\partial \zeta} \quad (17)$$

$$\begin{aligned} a_0 &= \frac{-v}{\delta \zeta + B} \\ a_1 &= \frac{w}{\sin \theta} \frac{1}{\delta \zeta + B} \\ a_2 &= \frac{1}{\delta} \left\{ u - \zeta \frac{\partial S}{\partial t} - \frac{1}{\delta \zeta + B} \left[v C(\theta) + \frac{w C(\phi)}{\sin \theta} \right] \right\} \\ a_3 &= \frac{\gamma}{\delta} \\ a_4 &= \frac{-\gamma}{\delta \zeta + B} \\ a_5 &= \frac{-\gamma}{\delta} \frac{C(\theta)}{(\delta \zeta + B)} \\ a_6 &= \frac{\gamma}{\sin \theta (\delta \zeta + B)} \\ a_7 &= \frac{-\gamma}{\delta} \frac{C(\phi)}{\sin \theta (\delta \zeta + B)} \\ a_8 &= \frac{\gamma(v \cot \theta + 2u)}{\delta \zeta + B} \\ a_9 &= \frac{1}{\delta} \frac{a^2}{\gamma} \\ a_{10} &= \frac{-(v^2 + w^2)}{\delta \zeta + B} \\ a_{11} &= \frac{-a^2}{\gamma (\delta \zeta + B)} \\ a_{12} &= \frac{-a^2}{\gamma \delta} \frac{C(\theta)}{(\delta \zeta + B)} \end{aligned} \quad (18)$$

$$a_{13} = \frac{uv - w^2 \cot \theta}{\delta \zeta + B}$$

$$a_{14} = \frac{a^2}{\gamma \sin \theta (\delta \zeta + B)}$$

$$a_{15} = \frac{-a^2}{\delta \gamma \sin \theta} \frac{C(\phi)}{(\delta \zeta + B)}$$

$$a_{16} = \frac{w}{(\delta \zeta + B)} \left\{ v \cot \theta + 2u - \frac{1}{\sin \theta} \right\}$$

This system of equations is numerically integrated with respect to time in the interior of the transformed computational space shown in Fig. 2b. The spatial derivatives appearing on the right-hand side of these equations are approximated by finite differences, and to do this, the continuous space of Fig. 2b is divided into a discrete three-dimensional grid of points as indicated in Fig. 2c. The space is first sectioned by cutting planes for equally spaced increments in the azimuthal angle ϕ , and up to nine such planes can be used in the present program. Each of these planes is then divided into a matrix of equally spaced points in the θ and ζ directions, and up to six points in ζ and 10 points in θ can be used. This spacing provides an indication of the complexity of the machine calculations when one considers that, as a minimum, values for each of the five dependent variables have to be stored for each of the possible 540 grid points. For an axisymmetric body at zero angle of attack, the grid equivalent of a single ϕ plane is required, and the solution of this case would always be more detailed in that more points could be stored, than in the more complex case with the body at an angle of attack.

With values of the variables assigned at each of the mesh points, the system of equations is numerically integrated with respect to the time to obtain new values at the interior field mesh points. The starting values for the integration are assumed, but vary with time under the influence of the applied boundary conditions.

McCormack's differencing scheme (Ref. 4) is used for the time-wise numerical integration. This method is a two-step method which has the advantage that while being of second order in accuracy, it does not require evaluation of second-order derivatives. The scheme is as follows. Let g represent the value of any of the dependent variables, $g_{i,j,k}^t$ represent the value of the variable at a time, t , at the

spatial position θ_i , ϕ_i , ξ_k . In the first step, a first estimate of the value of the variable at time $t + \Delta t$ is provided by

$$g_{i,j,k}^{t+\Delta t} = g_{i,j,k}^t + \Delta t \left(\frac{\partial g}{\partial t} \right) \quad (19)$$

The derivative in this equation is given by the right-hand side of the appropriate equation from Eqs. (13) through (17), with the spatial derivatives calculated using backward differences. Thus, for example, the difference approximation to the derivative $\partial g / \partial \theta$ is taken to be equal to

$$\left(g_{i,j,k}^t - g_{i-1,j,k}^t \right) / (\theta_i - \theta_{i-1})$$

In the second step, a revised estimate of the value of g at $t + \Delta t$ is given by

$$g_{i,j,k}^{t+\Delta t} = \frac{1}{2} \left\{ g_{i,j,k}^t + g_{i,j,k}^{t+\Delta t} + \Delta t \left(\frac{\partial g}{\partial t} \right) \right\} \quad (20)$$

The derivative in this expression is calculated as in the first step except that the estimates $g_{i,j,k}^{t+\Delta t}$ are used and a forward difference approximation to the spatial derivatives is used. The forward difference approximation of $\partial g / \partial \theta$ is given as

$$\frac{\left(g_{i+1,j,k}^{t+\Delta t} - g_{i,j,k}^{t+\Delta t} \right)}{(\theta_{i+1} - \theta_i)}$$

Note that since the second step uses differences of values calculated in the first step, the overall storage requirement is effectively doubled. This is the cost that is paid for retention of second-order accuracy without the calculation of second derivatives. Earlier versions of the Moretti analysis used a second-order Taylor series expansion for this time integration which did require second-order derivative calculations.

In performing the integration with respect to time, one cannot select the time increment arbitrarily, since it must satisfy the Courant-Friedrichs-Lewy (Ref. 4) stability criteria given as

$$\Delta t \leq \left(\frac{\Delta r}{u + a} \cdot \frac{r \Delta \theta}{u + a} \cdot \frac{r \sin \theta \Delta \phi}{u + a} \right) \quad (21)$$

where Δr , $r \Delta \phi$, $r \sin \theta \Delta \phi$ are the physical space mesh sizes and u and a are the total velocity and acoustic speed, respectively, at a grid point. Simply stated, for the calculation to be stable the time increment must be selected to be smaller than the smallest physical mesh dimension divided by the largest signal propagation speed at any of the grid points. In the present method, the time increment is taken to be two-thirds of the theoretical maximum value.

The application of this stability criterion leads to an important observation. If one should attempt to obtain a more detailed flow-field definition by halving the spatial increments, not only would the computational time increase due to the eightfold increase in the number of grid points (fourfold for the 2-D case), but also twice as many timewise integrations would be required to achieve the same asymptotic solution. It is also observed that the use of grid spacings which are nearly equal is efficient since the smallest grid spacing is the one that controls the time increment.

2.2 SHOCK POINTS

The points on the boundaries of the computational region are computed differently, and the shock boundary layer through which the free-stream nonuniformity enters will be considered first. Unfortunately, it is not possible to illustrate the four-dimensional space in which the calculation is carried out, so for purposes of illustration, the two-dimensional analog will be used. This model is also applicable to the angle-of-attack computation in the leeward and windward meridian planes where the shock curvature, in directions normal to these planes, is symmetric.

To illustrate the shock calculation, the physical system is illustrated in Fig. 3 for the leeward plane, $\phi = 0$. Consider that at time t the solution in the physical plane is known and, in particular, a point on the shock wave A_0 has a radial velocity, W . In the time interval Δt , the shock point moves a distance $W \Delta t$ and can be located at the point A in the $t + \Delta t$ plane. The position of A relative to the origin of the coordinate system determines the free-stream flow conditions upstream of the shock.

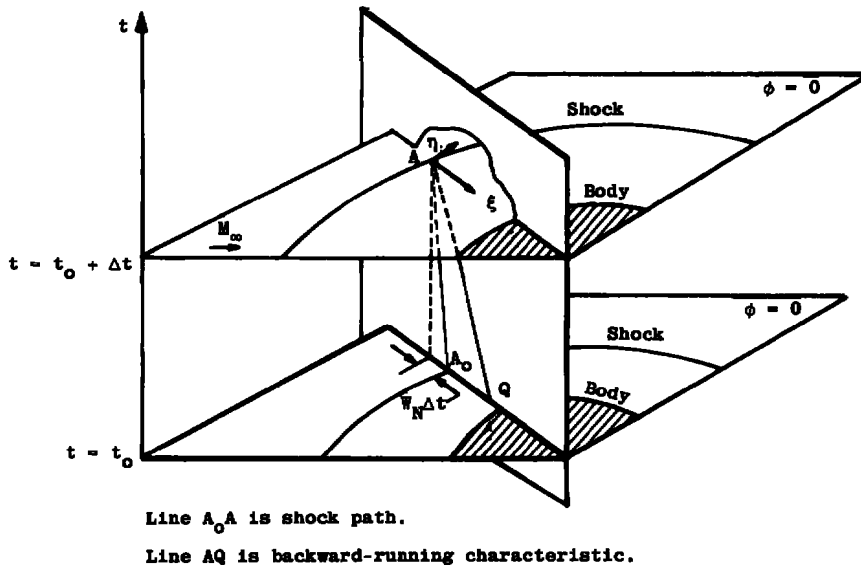


Figure 3. Diagram of geometry of the shock boundary calculation in the two-dimensional case or a symmetry plane calculation in the three-dimensional case.

At the point A let \vec{N} be an inward-directed vector normal to the shock surface and define an auxiliary cartesian coordinate system $(\vec{\eta}, \vec{\xi}, \vec{\tau})$ at A such that the unit vector $\vec{\xi}$ is parallel to \vec{N} and $\vec{\eta}$ is normal to $\vec{\xi}$ in the plane $\phi = \text{constant}$. The unit vector $\vec{\tau}$ is normal to $\vec{\xi}$ and $\vec{\eta}$. Further, let the velocity components in the directions $\vec{\xi}$, $\vec{\eta}$, $\vec{\tau}$ be given as \bar{u} , \bar{v} , and \bar{w} , respectively. The direction $\vec{\tau}$ and velocity \bar{w} are omitted from Fig. 3 for clarity.

It is well known that flow velocity components tangent to an oblique shock are unaltered by the shock while the normal component is changed in accordance with the Rankine-Hugoniot equations. Defining W_N as the component of the shock velocity in the direction \vec{N} and letting the subscripts 1 and 2 represent the conditions fore and aft of the shock at point A , the Rankine-Hugoniot conditions can be written as

$$\bar{v}_1 = \bar{v}_2, \quad \bar{w}_1 = \bar{w}_2$$

$$\bar{u}_2 = \frac{(\gamma - 1)(\bar{u}_1 - W_N)^2 + 2 a_1^2}{(\gamma + 1)(\bar{u}_1 - W_N)} + W_N$$

$$\frac{p_2}{p_1} = \frac{2\gamma(\bar{u}_1 - W_N)^2 - (\gamma - 1)}{\gamma + 1}$$

$$\frac{\rho_2}{\rho_1} = \frac{(\gamma + 1)(p_2/p_1) + (\gamma - 1)}{(\gamma + 1) + (\gamma - 1)p_2/p_1} \quad (22)$$

This is a system of five equations in the six unknowns; that is, the shock position is known, but the shock velocity is unknown. To provide the additional functional relation to complete the set, a quasi-one-dimensional analysis is employed. Consider a plane defined by the ξ - t coordinates as indicated in Fig. 3. In this plane the flow is considered to be quasi-one-dimensional, nonsteady flow under the assumption that the components of variable gradients tangent to the shock wave are constant.

The situation in the ξ , t plane is shown in Fig. 4. When the quasi-one-dimensional analysis is applied, it is found that there are three characteristics passing through the point A, given by

$$\frac{d\xi}{dt} = \bar{u} - a, \quad \frac{d\xi}{dt} = \bar{u} + a, \quad \frac{d\xi}{dt} = \bar{u} \quad (23)$$

and indicated in Fig. 4. The appropriate characteristic is the first one given, and the compatibility equation along this characteristic is given as

$$\frac{d\bar{u}}{dt} = \frac{a}{\gamma} \frac{dP}{dt} - \left(\bar{v} \frac{\partial \bar{u}}{\partial \eta} + w \frac{\partial \bar{u}}{\partial r} \right) + a \left(\frac{\bar{v}}{\gamma} \frac{\partial P}{\partial \eta} + \frac{\bar{w}}{\gamma} \frac{\partial P}{\partial r} + \frac{\partial \bar{v}}{\partial \eta} + \frac{\partial \bar{w}}{\partial r} \right) \quad (24)$$

This compatibility equation provides the additional relation which when added to the Rankine-Hugoniot relations results in a tractable set of nonlinear, algebraic equations which are solved by an iterative procedure. The iterative procedure is as follows:

1. Assume a value of the shock velocity W_N at point A in the $t + \Delta t$ solution plane.
2. Using the assumed shock velocity, evaluate the flow conditions behind the shock from the Rankine-Hugoniot relation, and, in particular, determine a value for \bar{u}_2 .
3. Construct the characteristic given by $d\xi/dt = \bar{u} - a$ and trace it back in time to the solution at time t_0 . Let the intercept be designated at Q as shown in Figs. 3 and 4.

4. Interpolate in the time = t_0 solution to determine the flow qualities and their derivatives at Q.
5. Using the values at point A from Step 2 and the values at Q from Step 4, integrate Eq. (6) from Q to A. This results in a new value of \bar{u}_2 at A.
6. Repeat Steps 1 through 5 until a shock velocity is found which causes the calculated values of \bar{u}_2 from Steps 2 and 5 to agree.

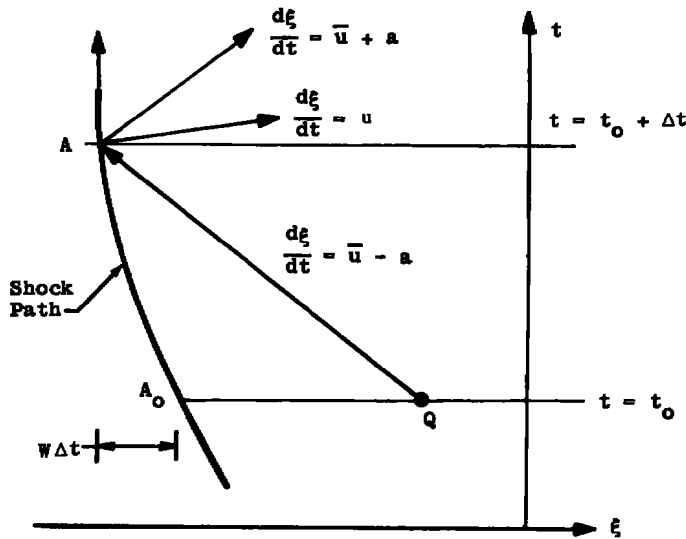


Figure 4. Shock path in the quasi-one-dimensional unsteady flow plane showing the three characteristic directions.

Since the free-stream nonuniformity enters into the solution through the shock-boundary calculations, some limitations on the allowable nonuniformities must be accepted. Obviously, the free-stream properties must be continuous. For example, the procedure would be incapable of handling a discontinuity in free-stream velocity such as a shear layer whose thickness is much smaller than the physical mesh size. In such a case one moving shock point could alternately pass in and out of the shear layer with a resulting cyclical instability. As indicated in Section 2.1, a reduction of the mesh size to account for such a locally steep gradient in the free stream would detract from the convergence due to the accompanying reduction in the allowable time increment.

It is assumed that by using the quasi-one-dimensional analysis in the shock calculation, one obtains gradients tangent to the shock which are small in comparison with the discontinuous changes normal to the shock. In the case of a uniform free stream, the gradients behind and tangent to the shock are due solely to the fact that the shock has a slowly varying radius of curvature. The presence of free-stream non-uniformities can change the curvature of the shock, and poor convergence might occur if the free-stream nonuniformity is concentrated where the shock experiences a rapid change in curvature (e.g., after the intercept with the sonic line). To summarize, the free-stream nonuniformities must generally be continuous and without large gradients so that significant variations do not occur over lengths comparable to the mesh size. The free-stream gradients should not be substantially larger than those resulting from shock curvature in the case of a uniform flow.

2.3 BODY POINTS

The calculation of the body boundary points is similar to the shock calculation, though simpler, since the entropy at the body is known and the normal component of the velocity vanishes. As in the shock computation, an auxiliary cartesian coordinate system defined by the unit vectors $\vec{\xi}$, $\vec{\eta}$, and $\vec{\tau}$ is defined but with $\vec{\xi}$ aligned normal to the body surface. The associated velocity components in the coordinate directions are again taken to be \bar{u} , \bar{v} , and \bar{w} , respectively. When the quasi-one-dimensional analysis is applied at the body, the appropriate characteristic is the one defined by

$$\frac{d\xi}{dt} = \bar{u} + a \quad (25)$$

in the ξ - t plane, as illustrated in Fig. 5. While \bar{u} is known to vanish at A, the acoustic velocity, a , is not known and must be initially guessed to construct the backward-running characteristic. Assuming a value for the acoustic velocity, the characteristic is constructed back to the previous time solution at the point Q where the flow variables are interpolated and transformed to the ξ , η , τ coordinate system. The appropriate compatibility equation along the $\bar{u} + a$ characteristic is given as

$$\frac{d\bar{u}}{dt} + \frac{a}{\gamma} \frac{dP}{dt} = - \left(\bar{v} \frac{\partial \bar{u}}{\partial \eta} + \bar{w} \frac{\partial \bar{u}}{\partial \tau} \right) - a \left(\frac{\bar{v}}{\gamma} \frac{\partial P}{\partial \eta} + \frac{\bar{w}}{\gamma} \frac{\partial P}{\partial \tau} - \frac{\partial \bar{v}}{\partial \eta} + \frac{\partial \bar{w}}{\partial \tau} \right) \quad (26)$$

The compatibility equation is approximated by a finite difference equation along the characteristic with the right-hand side evaluated at the point Q. This evaluation provides a value of the pressure P at point A. The calculated pressure and the known entropy determine the density at A as well as a new value for the acoustic velocity. An iterative procedure is performed until the resulting calculated acoustic velocity agrees with the value used to construct the characteristic.

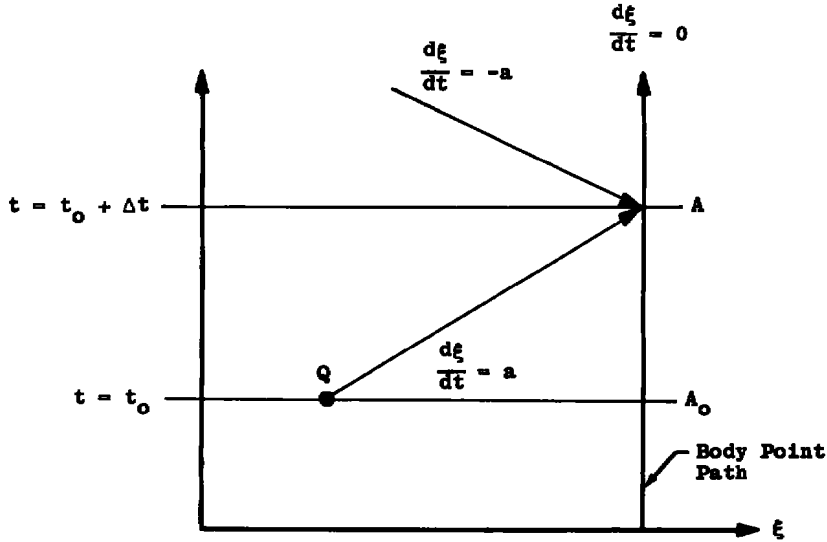


Figure 5. Body path in the quasi-one-dimensional unsteady flow plane showing the three characteristic directions with the condition that $\bar{u} = 0$ at the body surface.

After convergence of the iteration to determine the acoustic velocity at the body point, it is necessary to determine the velocity components \bar{v} and \bar{w} . These components are obtained from the two equations

$$-\frac{\partial \bar{v}}{\partial t} = \bar{v} \frac{\partial \bar{v}}{\partial \eta} + \bar{w} \frac{\partial \bar{v}}{\partial r} + \frac{p}{\rho} \frac{\partial P}{\partial \eta} = 0 \quad (27)$$

and

$$-\frac{\partial \bar{w}}{\partial t} = \bar{v} \frac{\partial \bar{w}}{\partial \eta} + \bar{w} \frac{\partial \bar{w}}{\partial r} + \frac{p}{\rho} \frac{\partial P}{\partial w} = 0 \quad (28)$$

again approximating the equations by finite differences. Equations (27) and (28) are simply the inviscid flow equations (3) and (4)

written in the η , ξ , τ cartesian coordinate system with the \bar{u} terms deleted on account of the fact that they vanish at the surface.

2.4 OUTER BOUNDARY

One does not have a priori knowledge of any of the boundary conditions along the surface $\theta = \theta_{\max}$ indicated in Fig. 2a. As a consequence, no boundary conditions are applied here. However, since this surface is totally comprised of supersonic flow, only those disturbances originating in the interior of the computational region can be propagated across this boundary. Therefore, the points on this surface are calculated by simple extrapolation with respect to the spatial variables. The extrapolation is carried out for each time solution generated, but the temporal derivatives of the variables at this surface never actually enter into the computational procedure.

In addition to the outlined boundary value calculations, there are certain extraneous conditions which should be noted. The computational planes $\phi = 0$ and $\phi = \pi$ are planes of symmetry so that derivatives with respect to ϕ vanish identically on these surfaces. The stagnation line is common to all of the ϕ planes and need only be calculated once. The stagnation line is taken to be a line of symmetry for the evaluation of derivatives normal to this line.

The present program is written for axisymmetric bodies generated from conic sections (circle, ellipse, paraboloid) with a conical aftbody. The extension to other shapes of revolution is straightforward; however, the surfaces must have continuous second-order partial derivatives. The restriction to axisymmetric bodies simplifies the calculations at the body boundary since the normal vector to the body always lies in the meridian planes. As pointed out, this occurs only in the windward and leeward planes in the case of the shock computation.

3.0 RESULTS OF SAMPLE CALCULATIONS

A solution to the blunt body problem in three spatial dimensions results in an extreme proliferation of numerical information which in itself represents a challenge to condense. It is possible to provide detail maps and to trace streamlines and surfaces of constant Mach

number, pressure, and density, but these are not of particular interest. However, certain gross results are of primary interest; these include shock shape, sonic line location, pressure distribution, and the rate of convergence to the solution. Only these gross characteristics will be discussed for a sample of cases run with the program.

All of the results presented are for a spherically blunt, 8-deg half-angle cone at a 3-deg angle of attack with a stagnation line, free-stream Mach number of 7. The results were obtained for seven ϕ planes with the grid in each ϕ plane having a total of 42 points, including the boundary points. The maximum azimuthal angle is 90 deg, and the coordinate system origin is located one-half nose radius behind the center of curvature of the spherical cap. For convenience, the results are presented in a conventional manner with the body azimuthal angle measured from the stagnation point.

Figure 6 depicts the flow field computation results in the pitch plane for a uniform free stream and illustrates the shock shape evolution with respect to the number of time iterations of the describing equations. As the figure illustrates, the initial guess of the shock shape was not very close; however, the estimate of the shock standoff distance was quite close. The reason for this apparently good guess is that it was made on the basis of data correlated for blunt cones at zero angle of attack and does not change much for small angles of attack.

The results of Fig. 6 indicate that the evolution of the shock shape is quite rapid, with an indistinguishable difference between the results of 200 and 300 time steps for the scale used in the figure. The final shock shape in Fig. 6 is not symmetric with respect to the body and is closer to the body in the lower, windward half plane.

As an example of a nonuniform flow calculation, the free-stream nonuniformity was taken to be a flow having a centerline Mach number of 7 and an outer flow Mach number of 14. The velocity distribution was assumed to be a sine function over a distance of two nose radii normal to the stagnation line. Profiles of the density, velocity, and flow Mach number, referenced to the centerline values, for the non-uniform free stream are indicated in Fig. 7. As indicated in Fig. 7, the resulting velocity variation is only on the order of 4 percent. However, the gradients in Mach number and density are substantial. In addition, since the free-stream static pressure is constant, the

indicated variation in Mach number implies an order of magnitude variation in the free-stream total pressure.

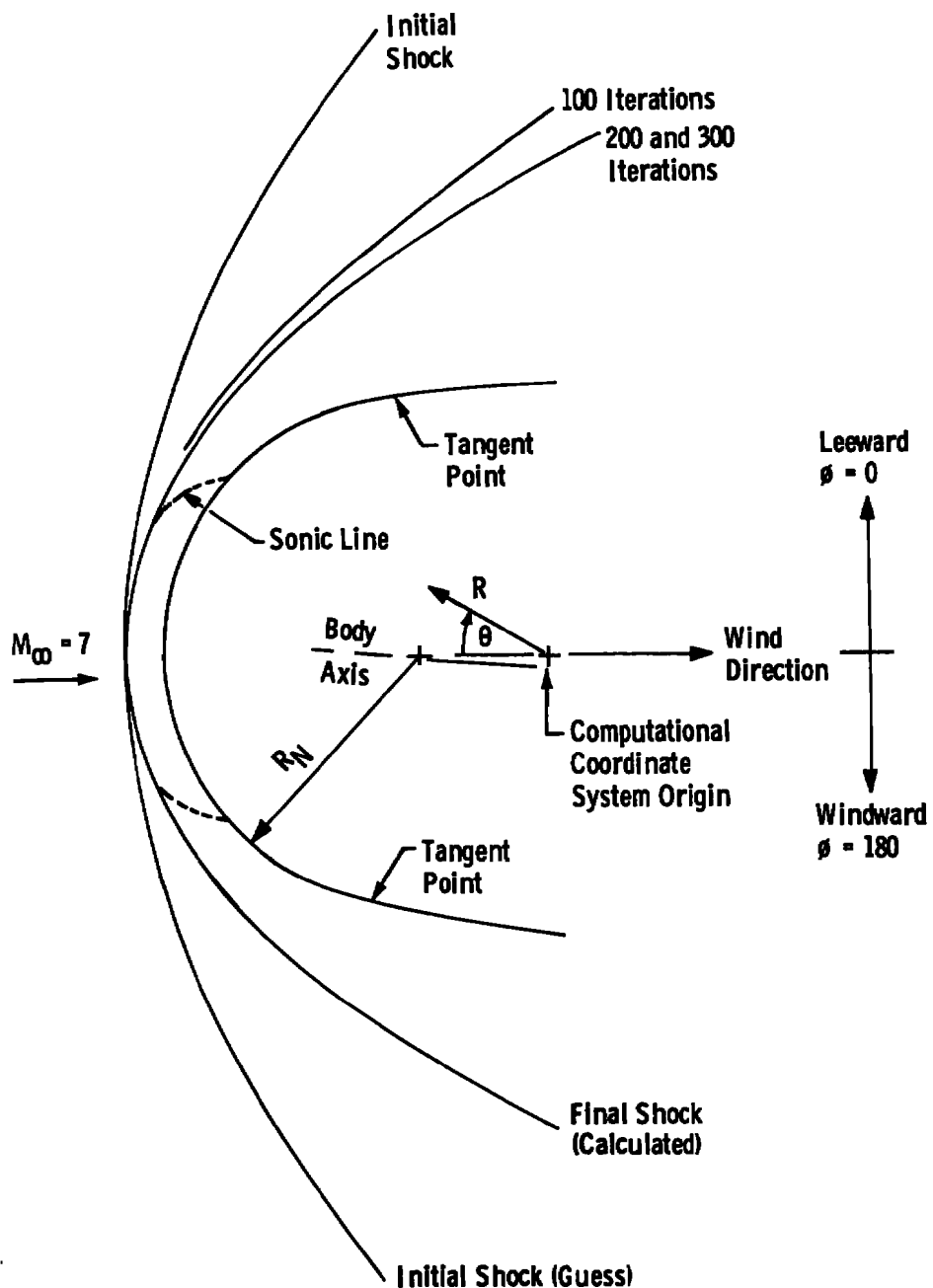


Figure 6. Three-dimensional flow field for an 8-deg sphere cone at 3 deg angle of attack in a Mach number 7.0 uniform flow.

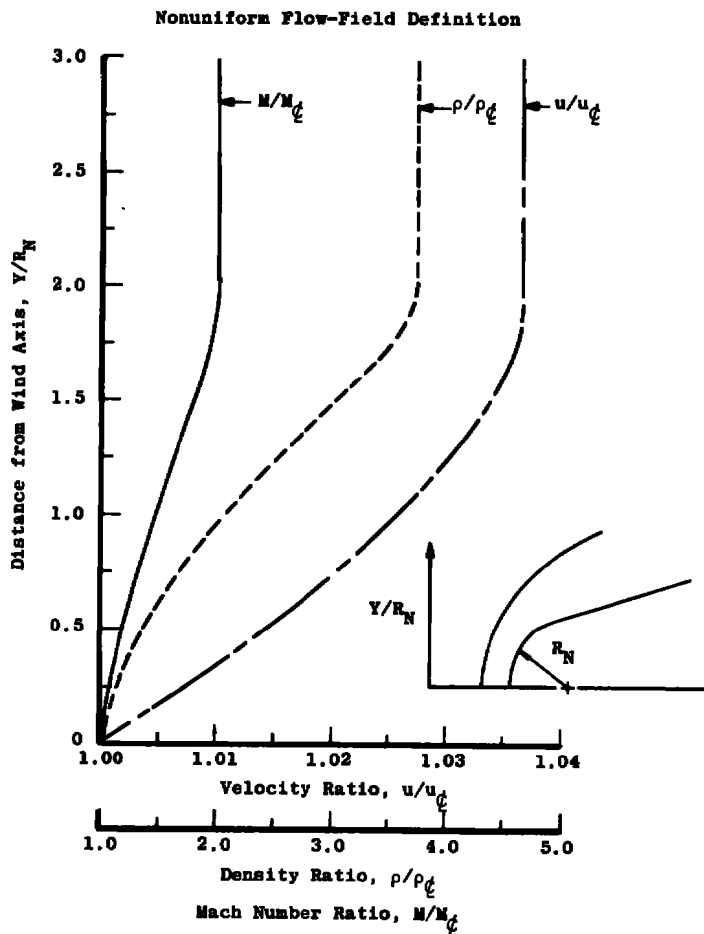


Figure 7. Nonuniform free-stream model used to illustrate effects of a radially increasing flow Mach number.

In Fig. 8, the resulting shock geometry calculated for the free-stream nonuniformity of Fig. 7 is presented. The shock shape of the uniform flow calculation (Fig. 6) is also shown in Fig. 8 for comparison. In comparing the shapes, one finds that the result for the nonuniform flow has a smaller radius of curvature, as would be anticipated by virtue of the higher free-stream Mach number. By the same reasoning, one would expect that the shock standoff distance would also be decreased in the case of the nonuniform flow, although the results indicate the contrary. It is also possible to make a qualitative comparison of the sonic lines in Fig. 8 with those of Fig. 6. For the nonuniform flow model used, the sonic lines are straighter. The sonic line intercepts with the body occur at nearly the same locations for both the uniform and nonuniform cases.

However, the intercept of the sonic line with the shock occurs closer to the coordinate axis in the case of the nonuniform flow. This can be a Mach number effect indicative of a steeper velocity gradient behind the shock.

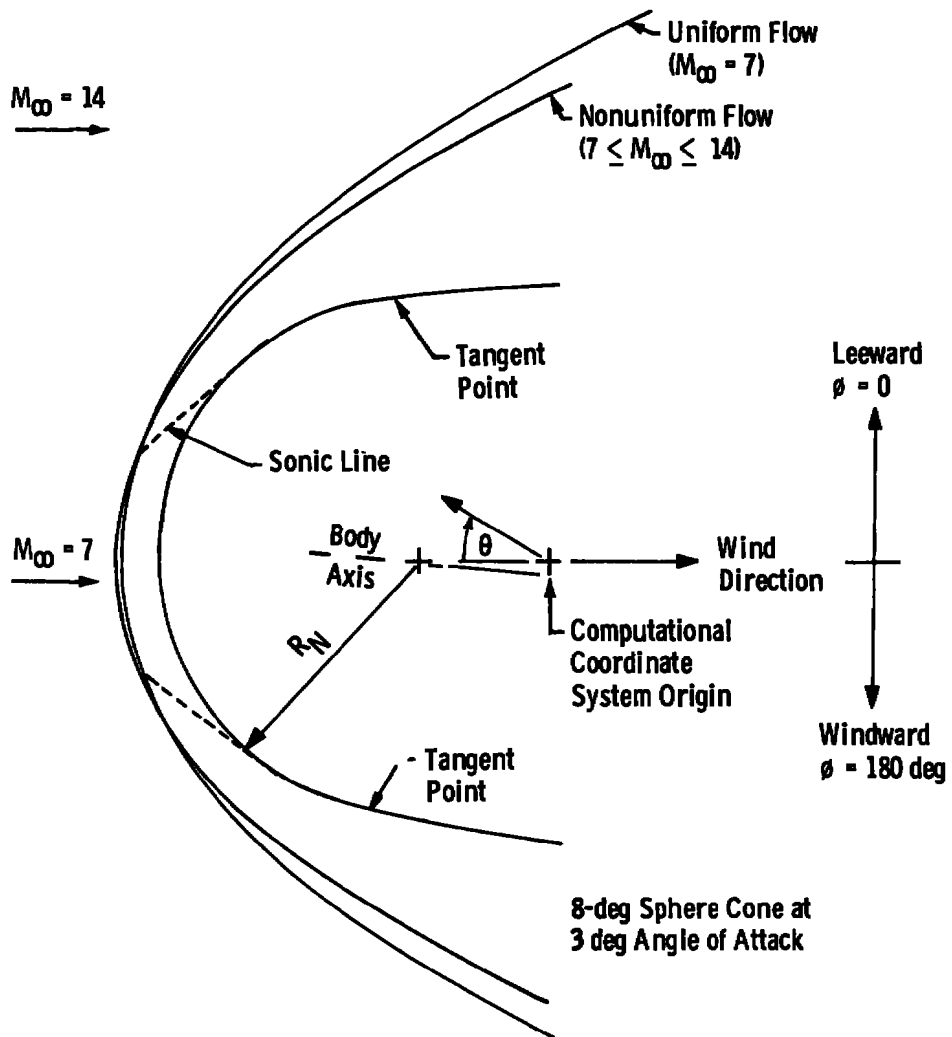


Figure 8. Calculated shock shape for a nonuniform free-stream flow in which the Mach number radially increases.

In Fig. 9, the resulting static pressure distributions along the body surface are presented for the uniform and nonuniform computations. The pressure distributions are given for the windward ($\phi = 180$ deg), side ($\phi = 90$ deg), and leeward ($\phi = 0$) half planes.

Individually, the pressure distributions for the uniform flow case appear reasonable and self-consistent in that the pressures decrease monotonically with the azimuthal angle and result in higher values in the windward plane than in the leeward plane. The increased pressures for the nonuniform case as well are consistent with intuition since the free-stream total pressure of the nonuniform case is larger than that of the uniform case.

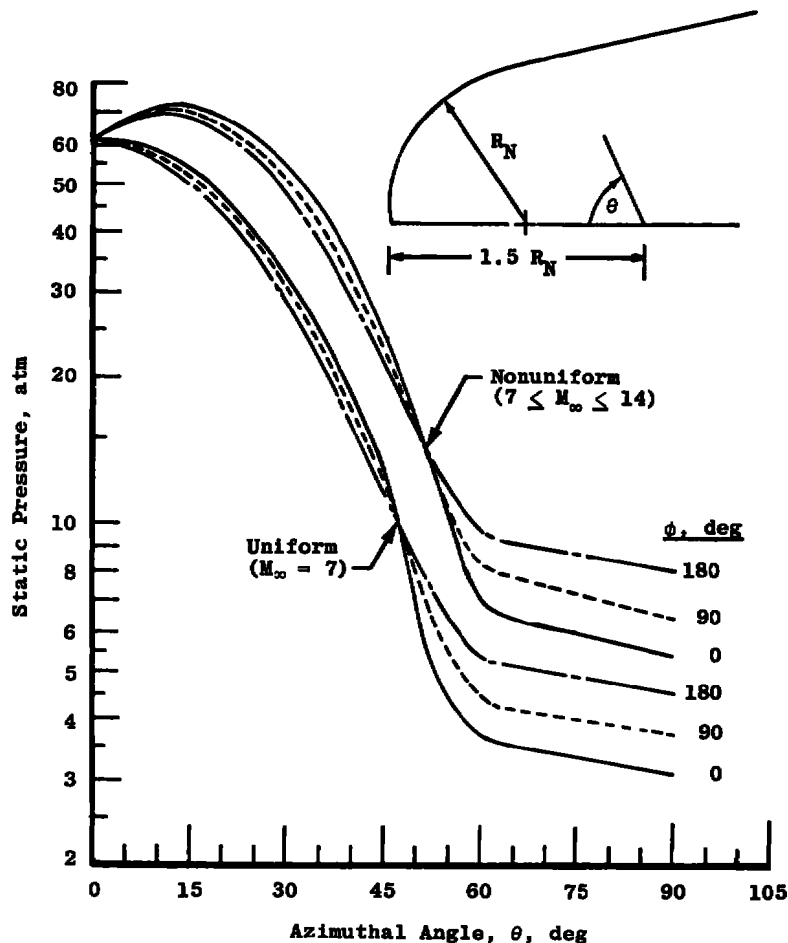


Figure 9. Calculated static pressure distributions for a uniform free stream and nonuniform free stream in which the Mach number radially increases.

Of particular concern, however, is the pressure overshoot near the stagnation point for the nonuniform flow. It would appear that such an overshoot is not valid and may be attributed to a poor definition of the flow field or a violation of the assumption that the stagnation line

lies on the coordinate axis. On the other hand, in support of the existence of such an overshoot, the results for all the variables are consistent. The velocity distributions in the vicinity of the stagnation point are shown in Fig. 10, and the indicated reduction in the velocity in the case of the nonuniform flow appears consistent with the pressure increase shown in Fig. 9. In contrast to the earlier discussion of the sonic line shape for the nonuniform flow, the results indicate that the velocity gradients behind the shock are increased, but are reduced at the body as a consequence of the nonuniformity in the free stream.

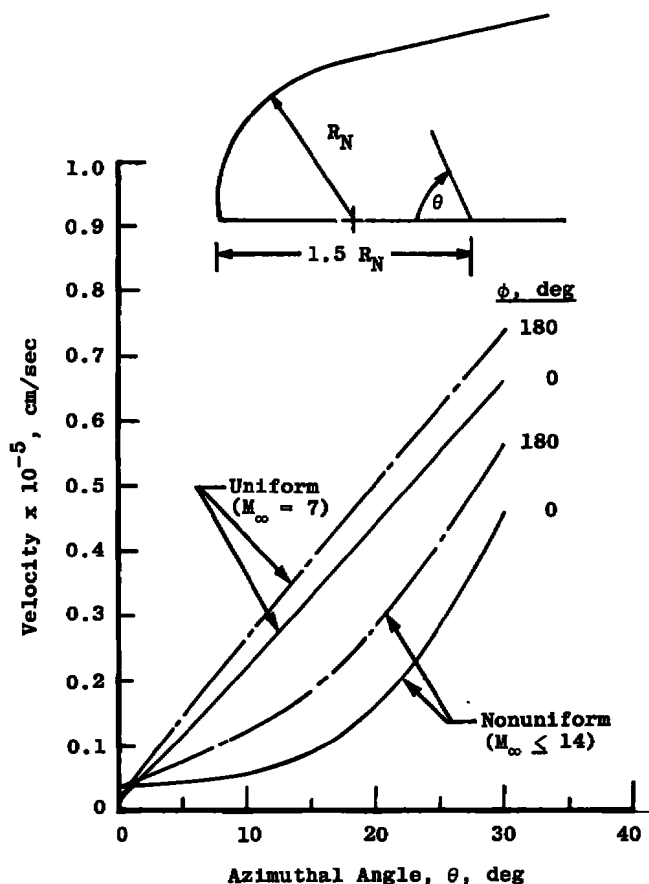


Figure 10. Calculated flow velocities near the body stagnation point for a uniform free stream and a nonuniform free stream in which the Mach number radially increases.

If this is indeed the case, it can have a significant impact on the interpretation of experimental stagnation point heating rates. Stagnation point heating rates are directly proportional to the square root of

the velocity gradient, and the velocity gradient for a uniform flow is inversely proportional to the nose radius. This is not true for a nonuniform flow, and simple correlation of stagnation point heating with nose radius may not be valid.

The flow nonuniformity can also be reversed in the sense that the outer flow Mach number can be less than the centerline value. Results of such a computation with the outer Mach number assumed to be 5 are shown in Figs. 11 through 14. The velocity distribution was assumed to be a sine function, as described previously. In addition to the noticeable changes in the sonic lines, the shock wave shape that results exhibits a noticeable change in curvature. This results from the nonmonotonic variation of the shock curvature. It

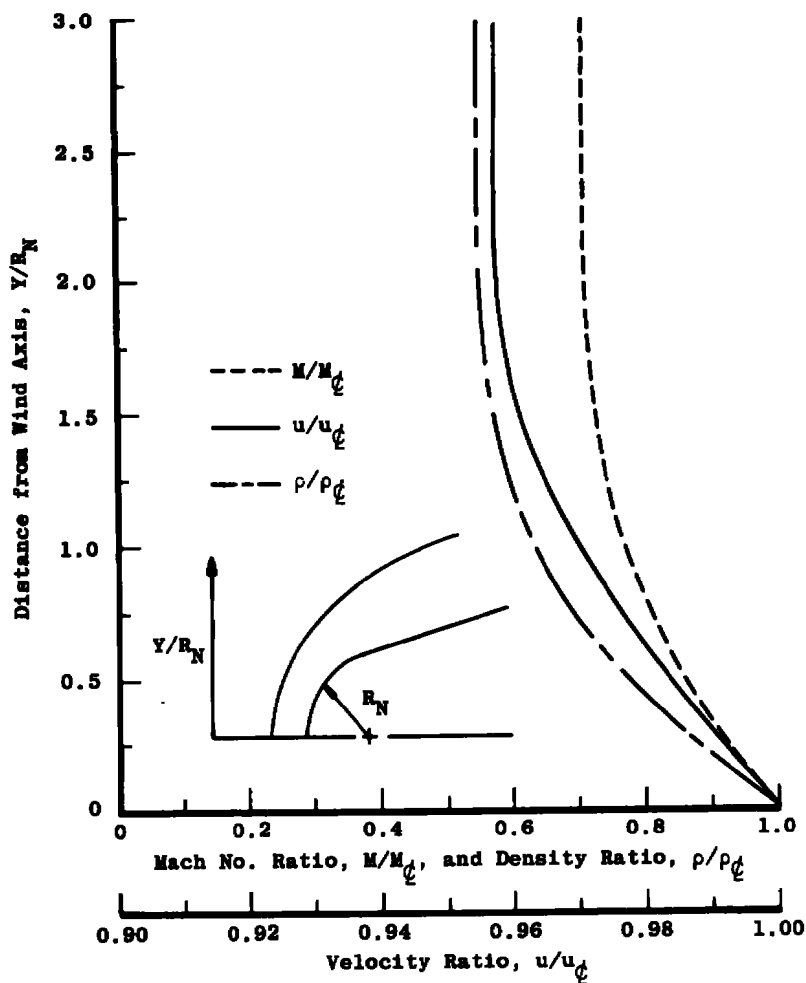


Figure 11. Nonuniform free-stream model used to illustrate effects of a radially decreasing flow Mach number.

would be expected that if the outer flow Mach number were reduced too much the sonic flow would extend outward to the point where it would not be possible to retain a reasonable mesh size and satisfy the criterion that the flow across the closure surface be supersonic. Finally, it is noted that the solution is, in fact, opposite to that of the case previously presented in that the stagnation point pressures were lowered (Fig. 13) and the velocity gradients increased over those of the uniform flow case (Fig. 14).

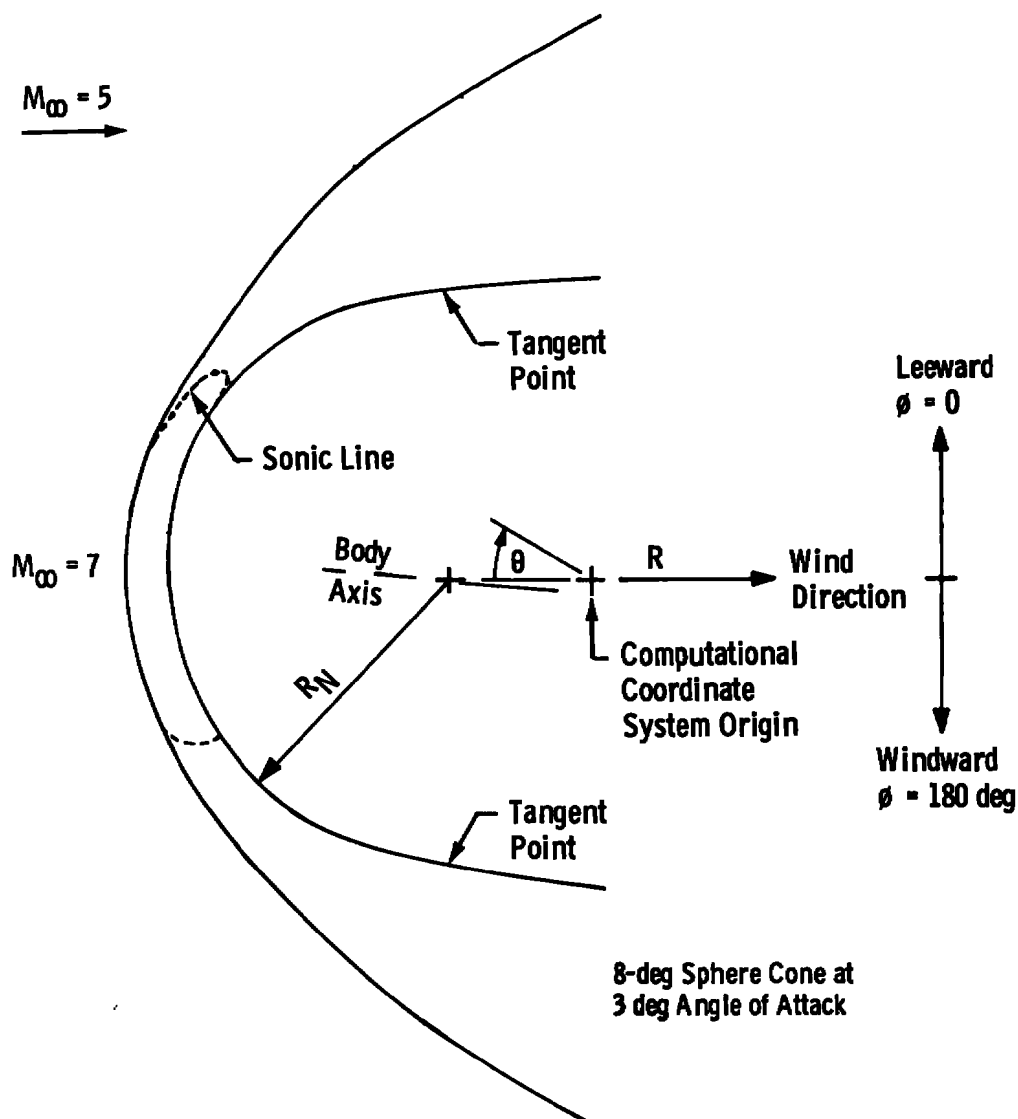


Figure 12. Calculated shock shape for a nonuniform free-stream flow in which the Mach number radially decreases.

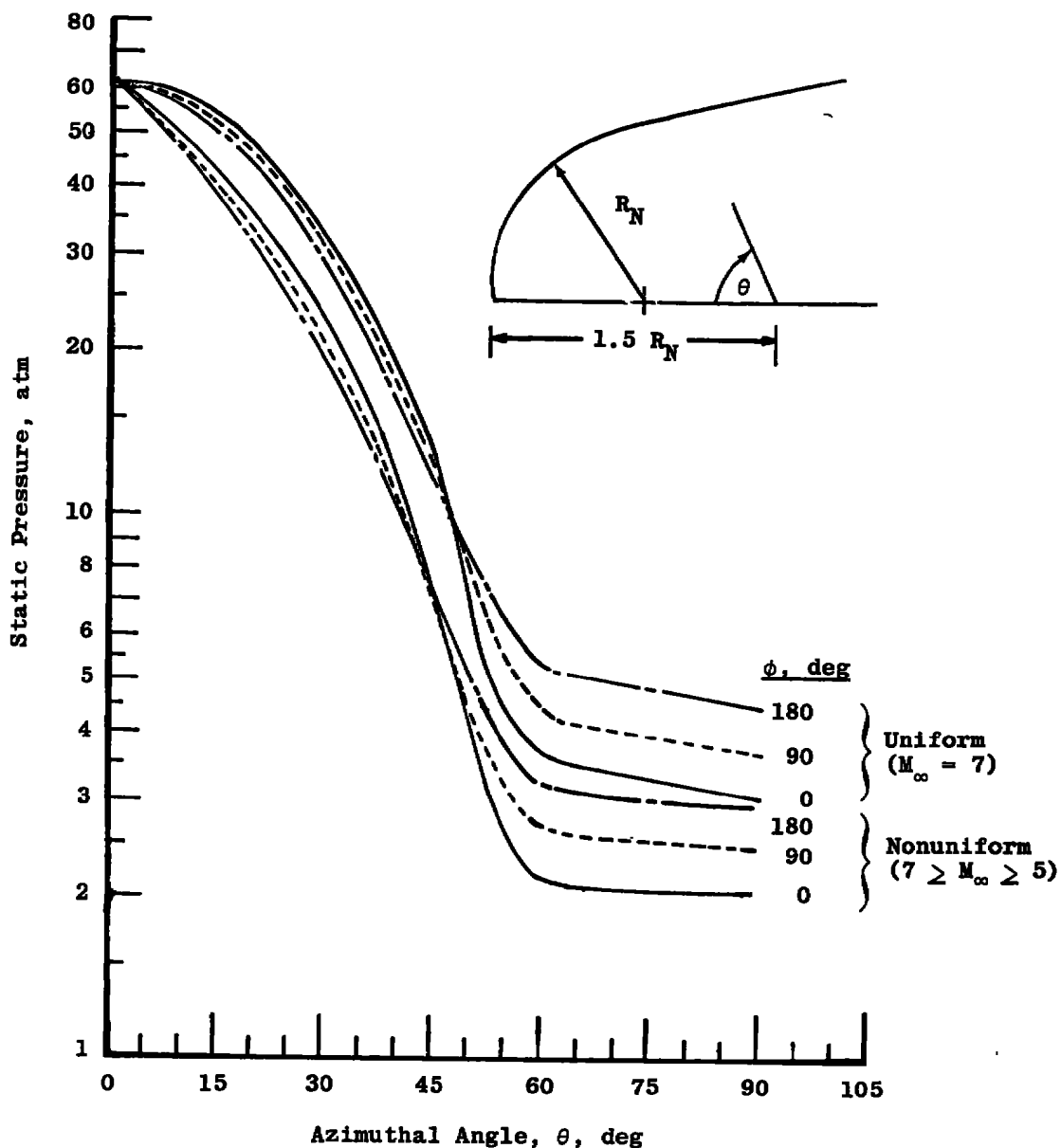


Figure 13. Calculated static pressure distributions for a uniform free stream and a nonuniform free stream in which the Mach number radially decreases.

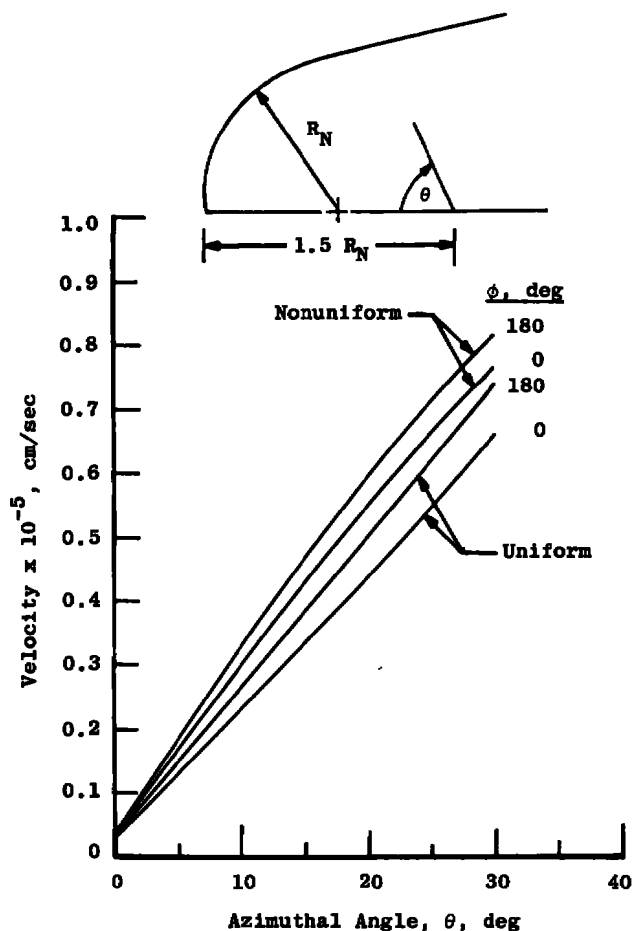


Figure 14. Calculated flow velocities near the body stagnation point for a uniform free stream and a nonuniform free stream in which the Mach number radially decreases.

4.0 CONCLUSIONS

The primary conclusion to be drawn from this study is that a free-stream nonuniformity of the type considered can indeed have a significant effect on the results obtained from model tests in such an environment. In particular, the free-stream effects must be properly accounted for when one is correlating or comparing experimental data from different sources. A second conclusion which the results support is that the concept of simulating the pressure distribution around a model by the use of a shrouded flow is viable. The

results support the observation that Moretti's time-dependent method, originally created as a design tool in uniform flows, has a potential for significant utilization in experimental investigations where the desirable flow uniformity is difficult to achieve.

In its present form, the programmed analysis restricts the form of the allowable nonuniform free-stream definition to be axially symmetric about a body stagnation line. In addition to this restriction, there are additional restrictions for which no firm guidelines can be established. Thus, one has to take into consideration the interrelations between the free-stream Mach number, the grid dimensions, the coordinate region, and the gradient in the free stream when formulating a problem. Many of these aspects have been considered in the appropriate preceding sections; however, fuller understanding of and familiarity with the constraints comes only with application to problems of interest.

The flow Mach number is of primary importance in the calculation. Indeed, as pointed out, the mathematical character of the describing steady-state flow equations can be elliptic or hyperbolic depending on whether the Mach number is less than or greater than unity. Generally, the numerics of the computation become more inherently stable with increasing free-stream Mach number. This results from the stability criteria as well as the fact that the flow tends to be asymptotic in Mach number. In other words, two flow geometries for free-stream Mach numbers of 10 and 12, for example, are physically quite similar; more so than two flows having Mach numbers of 2 and 3.

For a uniform free stream, experience has shown that the solution starts to exhibit poor convergence to the asymptotic limit as the Mach number approaches 1.5. For a nonuniform free stream, this limit can serve as a guideline, but no further firm criteria can be established. For example, it can be expected that for a free stream in which the Mach number varies over the range from 2.0 to 2.5, a solution can be readily obtained. On the other hand, if the variation is over the range from 2.0 to 10.0, the method would break down as a consequence of the other large gradients in the free stream.

Certainly in the case of zero angle of attack (two dimensions) and possibly in the case of a finite angle of attack, the calculation can be extended further downstream on the body using conventional steady flow analytical methods. At the present time, such an extension, while of academic interest, would not be applicable to any known practical application.

The present method is also incapable of accounting for discontinuities such as thin shear layers or impinging shocks in the free stream. Such surfaces would actually be additional boundary value surfaces. It would appear that such phenomena could be considered on an individual basis, but such consideration would require a complete reformulation of the analysis.

A basic assumption in the method is that the stagnation streamline is straight, parallel to the free-stream wind direction, and normal to the bow shock wave. This assumption permits the steady normal shock entropy to be assigned to the body surface. In a uniform free stream, this assumption is valid only if the body surface in the subsonic region of the flow field is symmetric about the stagnation streamline. This does not require that the body be axisymmetric; however, spherically blunted shapes which are of common interest always satisfy this requirement as long as the angle of attack is such that the subsonic flow field does not extend beyond the spherical cap. In the case of a nonuniform free stream, the validity of the above assumption additionally requires that the free-stream properties have a similar symmetry about the stagnation streamline. In the present calculation, the axisymmetric model of the nonuniform free stream is representative of the situation one would expect to exist in conventional aerodynamic testing devices. For more general tip shapes or flow nonuniformities, the assignment of the body entropy at the body surface would be an approximation, and results based on the method would have to be considered accordingly.

REFERENCES

1. Moretti, G. and Abbett, M. "A Fast, Direct, and Accurate Technique for the Blunt Body Problem, Part I - Analysis." Technical Report 583, General Applied Science Laboratories, Inc., June 1966.
2. Moretti, G. and Bleich, G. "Three-Dimensional Flow Around Blunt Bodies." AIAA Journal, Vol. 5, No. 9, September 1967, pp. 1557-1562.
3. Abbett, M.J. and Fort, R. "Three-Dimensional Inviscid Flow About Supersonic Blunt Cones at Angle of Attack, III: Coupled Subsonic and Supersonic Programs for Inviscid Three-Dimensional Flow." Sandia Laboratories Report SC-CR-68-3728, September 1968.

4. MacCormack, R. W. "The Effect of Viscosity in Hypervelocity Impact Cratering." AIAA Paper No. 69-354, April 1969.
5. Courant, R., Friedrichs, K. O., and Lewy, H. "Über die partiellen Differenzengleichungen der Mathematischen Physik." Math. Annual, Vol. 100, p. 32, 1928.

NOMENCLATURE

a	Speed of sound, cm/sec
$a_0 \dots a_{15}$	Coefficients in governing flow equations
B	Function defining body surface
C	Auxiliary function defined by Eq. (7)
E	Nondimensional entropy, $E = P - \gamma R$
g	Dummy notation for a dependent variable
i, j, k	Indices for spatial grid in ϕ , θ , ξ space
M	Mach number
P	Nondimensional pressure = $\ln(p/p_\infty)$
p	Static pressure, dynes/cm ²
p_∞	Free-stream static pressure, dynes/cm ²
R	Nondimensional density = $\ln(\rho/\rho_\infty)$
r	Radial coordinate, cm
r_n	Body nose radius, cm
S	Implicit function defining shock surface
s	Entropy
T	Transformed time, t
t	Nondimensional time
t_∞	Time reference, $t_\infty = r_n / \sqrt{(p_\infty/\rho_\infty)}$
u, v, w	Nondimensional velocity components in ξ, θ, ϕ space
$\bar{u}, \bar{v}, \bar{w}$	Nondimensional velocity components in the auxiliary $\bar{\eta}, \bar{\tau}, \bar{\xi}$ reference frame

u_r, u_θ, u_ϕ	Velocity components in physical space, cm/sec
W	Shock velocity in radial direction, cm/sec
W_N	Shock velocity component in $\vec{\xi}$ direction
x	Dummy functional argument
α	Angle of attack, deg
γ	Ratio of specific heats = 1.4
$\Delta t, \Delta \xi, \Delta \theta, \Delta \phi$	Grid spacing in computational space
δ	Distance along r between shock and body
ξ	Nondimensional transformed radial coordinate = $(r - B)/\delta$
$\vec{n}, \vec{\tau}, \vec{\xi}$	Vectors defining an auxiliary cartesian coordinate system
Θ	Transformed azimuth angle = θ
θ	Coordinate azimuth angle, radians
θ_{\max}	Maximum azimuth angle as measured from wind vector
ρ	Flow density, gm/cc
$\rho_\infty \zeta$	Free-stream flow density on stagnation streamline, gm/cc
Φ	Transformed coordinate meridian angle = ϕ
ϕ	Coordinate meridian angle, radians

SUBSCRIPTS

1, 2	Conditions fore and aft of shock in Rankine Hugoniot relations
ζ	Free-stream stagnation streamline value
i, j, k	Indices for grid in θ, ϕ, ξ space
r, θ, ϕ	Physical coordinate directions
∞	Free-stream value